



# Revisiting the Indian summer monsoon–ENSO links in the IPCC AR4 projections: A cautionary outlook

Mathew Roxy, Nitin Patil, K. Aparna, Karumuri Ashok\*

Centre for Climate Change Research, Indian Institute of Tropical Meteorology, Pune, India

## ARTICLE INFO

### Article history:

Received 27 March 2012

Accepted 11 February 2013

Available online 17 February 2013

### Keywords:

ENSO Modoki

ENSO - Indian monsoon teleconnections  
climate change

## ABSTRACT

The climate change experiments under the fourth Assessment Report (AR4) of the Intergovernmental Panel on Climate Change (IPCC), namely the twentieth century simulations (20C3M) and Special Report on Emissions Scenarios (SRES) A1B, are revisited to study whether these models can reproduce the ENSO and ENSO Modoki patterns as the two important modes from statistical linear analysis as observed. The capability of the models in simulating realistic ENSO/ENSO Modoki teleconnections with the Indian summer monsoon, and also the implications for the future are also explored. Results from the study indicate that only ~1/4th of the models from 20C3M capture either ENSO or ENSO Modoki pattern in JJAS. Of this 1/4th, only two models simulate both ENSO and ENSO Modoki as important modes. Again, out of these two, only one model simulates both ENSO and ENSO Modoki as important modes during both summer and winter.

It is also shown that the two models that demonstrate ENSO Modoki as well as ENSO associated variance in both 20C3M and SRESA1B represent the links of the ISMR with ENSO reasonably in 20C3M, but indicate opposite type of impacts in SRESA1B. With the limited skills of the models in reproducing the monsoon, the ENSO and ENSO Modoki, it is difficult to reconcile that the teleconnections of a tropical driver can change like that. All these indicate the challenges associated with the limitations of the models in reproducing the variability of the monsoons and ENSO flavors, not to speak of failing in capturing the potential impacts of global warming as they are expected to. More research in improving the current day simulations, improving model capacity to simulate better by improving the Green House Gases (GHG) and aerosols in the models are some of the important and immediate steps that are necessary.

© 2013 Elsevier B.V. All rights reserved.

## 1. Introduction

The El Niño–Southern Oscillation (ENSO) is an important source of interannual variability of the Indian summer monsoon (Rasmusson and Carpenter, 1983; Ropelewski and Halpert, 1987; Shukla, 1987). Since the last few decades, in association with a changing climate, the ocean heat content, and in turn the tropical Pacific SST is also changing (Levitus et al., 2005; Ashok et al., 2007). Recent studies point out the existence of a new phenomenon, referred to as the El Niño Modoki, characterized by warm SST anomaly in the central equatorial Pacific and cold SST anomaly in the western and eastern Pacific (Ashok and Yamagata, 2009; Kao and Yu, 2009; Kug et al., 2010). Studies argue that the increasing frequency of the El Niño Modoki in the recent decades is due to global warming (Ashok et al., 2007; Yeh et al., 2009). As a result, the maximum SST anomaly (SSTA) is found to persist in the central Pacific from the boreal summer through to the winter, modifying the atmospheric circulation and resulting indistinctly different

global impacts. In this context, it is imperative to examine the changing scenario of teleconnection between ENSO/Modoki and the Indian summer monsoon.

Towards the fourth Assessment Report (AR4) of the Intergovernmental Panel on Climate Change (IPCC), climate modeling groups have performed a well-coordinated set of twentieth century simulations (20C3M) and Special Report on Emissions Scenarios (SRES) A1B climate change experiments (Kripalani et al., 2007). These simulations using the state-of-the-art coupled ocean–atmosphere models are purportedly well suited for diagnosing the El Niño patterns (AchutaRao and Sperber, 2006; Collins et al., 2006) and its teleconnections such as those with Indian summer monsoon rainfall (Annamalai et al., 2007; Kripalani et al., 2007; Roxy et al., 2011; Sabade et al., 2011) in a global warming scenario and by analogy, to diagnose the monsoon–Modoki links. Interestingly, most of the studies that examine the monsoon teleconnections mainly compare the variability of an ENSO index such as the Niño3 with the observations for the 20 century. However, given the recent findings on the changing structures of the tropical Pacific SST modes, on which the teleconnections depend, reproduction of the distinct modal patterns is very important. Therefore, the primary objectives of the current study are: (1) to examine whether the AR4 climate models can reproduce the El Niño and El Niño Modoki patterns as the

\* Corresponding author at: Centre for Climate Change Research, Indian Institute of Tropical Meteorology, Pune 411008, India.

E-mail address: [ashok@tropmet.res.in](mailto:ashok@tropmet.res.in) (K. Ashok).

gravest two statistical modes of the tropical Pacific SST variability, (2) to evaluate the fidelity of the respective teleconnections of the El Niño and El Niño Modoki phenomena with Indian Summer Monsoon Rainfall (ISMR) and (3) to assess the future projections of the monsoon-ENSO (or ENSO Modoki) in SRESA1B simulated by the ‘better’ models.

Data sets and the statistical methodologies used are described in Section 2, and the results are discussed in Section 3. The study is summarized in Section 4.

## 2. Model description and data

SST and precipitation from the twentieth century simulations (20C3M) and Special Report on Emissions Scenarios (SRES) A1B scenario climate change runs performed by various modeling groups within the World Climate Research Program (WCRP) Coupled Model Inter-comparison Project phase 3 (CMIP 3; see Meehl et al., 2007; refer Table 1 for the model details) have been used in this study. The twentieth century climate change represented by the acronym simulations, carried out from the year 1901 to 2000, with anthropogenic and natural forcings (20C3M) is deemed as the control run. The ‘climate change’ impacts are evaluated by comparing the results from the control run with corresponding results from a 100 years climate change projection (SRESA1B) run, in which the concentration of CO<sub>2</sub> is fixed to ~700 ppm. The last 30 years in the 20C3M and SRESA1B scenario are used for the comparison.

The results for the boreal summer season (June–September; JJAS) are chiefly examined, to which the Indian summer monsoon is phase locked. However, the evolution of ENSO and ENSO Modoki variability for the winter season is also diagnosed while evaluating the fidelity of these events, for the boreal winter season (December–February; DJF). The Nino3 and the El Niño Modoki indices (EMI; Ashok et al., 2007) are prepared for representing the climate variability over the tropical pacific, viz. ENSO and Modoki. The definitions of the two indices are as follows:

$$\text{Nino3} = [\text{SSTA}]_{\text{EP}},$$

where  $[\text{SSTA}]_{\text{EP}}$  is the SSTA averaged over the tropical eastern Pacific (EP; 150°W–90°W, 5°S–5°N), and

$$\text{EMI} = [\text{SSTA}]_{\text{A}} - 0.5 * [\text{SSTA}]_{\text{B}} - 0.5 * [\text{SSTA}]_{\text{C}},$$

where  $[\text{SST}]_{\text{A}}$ ,  $[\text{SST}]_{\text{B}}$ , and  $[\text{SST}]_{\text{C}}$  stand for the averaged SSTA over the regions A (165°E–140°W, 10°S–10°N), B (110°W–70°W, 15°S–5°N), and C (125°E–145°E, 10°S–20°N), respectively.

In order to assess the capability of the models in reproducing the observed climate variability, we compare the simulations with (1) the global SST datasets from the Hadley Centre (HadISST; Rayner et al., 2003) and (2) the gridded observational rainfall dataset for the Indian subcontinent (Rajeevan et al., 2006). The HadISST analysis is based on in situ and, when available, satellite-based observations. The gridded rainfall dataset is based on rainfall data from 1803 stations each with at least 90% data availability.

## 3. Results

### 3.1. ENSO, ENSO Modoki and the Indian monsoon in the observations and the 20C3M simulations

An EOF analysis (Bretherton et al., 1992) is applied on the observed SST datasets to identify the prominent modes of climate variability for the boreal summer (JJAS) and winter (DJF) seasons during the period 1971–2000. Similar analysis is applied on the IPCC 20C3M datasets from 23 coupled models for the last 30 years of simulation to explore whether these models can reproduce the modal features of the ENSO and ENSO Modoki.

The EOF1 (Fig. 1a) portrays the prominent ENSO pattern (Rasmusson and Carpenter, 1982; McPhaden et al., 1988), as seen by the pattern as well as the strong correlation of 0.95 between the PC1 (Fig. 1c) and Nino3 index (Figure not shown), which is significant at 99% confidence level from a two tailed Student’s t-test. This mode explains about 44.8% of the SST variance for the boreal summer season, for the period under consideration. The EOF2 explains 14.8% of the SST variability and is associated with the slow change in the background gradient attributed to

**Table 1**  
Climate models available in the WCRP CMIP3 dataset.

Originating group(s)	Country	CMIP3 I.D.	Atmosphere (resolution)	Ocean (resolution)
Beijing Climate Center	China	BCC-CM1	T63 (1.9° × 1.9°) L16	(1.9° × 1.9°) L30
Bjerknes Centre for Climate Research	Norway	BCCR-BCM2.0	T63 (1.9° × 1.9°) L31	(0.5°–1.5° × 1.5°) L35
Canadian Centre for Climate Modeling & Analysis	Canada	CGCM3.1(T47)	T47 (–2.8° × 2.8°) L31	(1.9° × 1.9°) L29
Canadian Centre for Climate Modeling & Analysis	Canada	CGCM3.1(T63)	T63 (–1.9° × 1.9°) L31	(0.9° × 1.4°) L29
Météo-France/Centre National de Recherches Météorologiques	France	CNRM-CM3	T63 (–1.9° × 1.9°) L45	(0.5°–2° × 2°) L31
CSIRO Atmospheric Research	Australia	CSIRO-Mk3.0	T63 (–1.9° × 1.9°) L18	(0.8° × 1.9°) L31
CSIRO Atmospheric Research	Australia	CSIRO-Mk3.5	T63 (–1.9° × 1.9°) L31	(1.5° × 1.5°) L40
Max Planck Institute for Meteorology	Germany	ECHAM5/MPI-OM	T30 (–3.9° × 3.9°) L19	(0.5°–2.8° × 2.8°) L20
Meteorological Institute of the University of Bonn, Meteorological Research Institute of KMA, and Model and Data group.	Germany/ Korea	ECHO-G	T42 (–2.8° × 2.8°) L26	(1.0° × 1.0°) L16
US Dept. of Commerce/NOAA/Geophysical Fluid Dynamics Laboratory	USA	GFDL-CM2.0	(2.0° × 2.5°) L24	(0.3°–1.0° × 1.0°)
US Dept. of Commerce/ NOAA/ Geophysical Fluid Dynamics Laboratory	USA	GFDL-CM2.1	(2.0° × 2.5°) L24	(0.3°–1.0° × 1.0°)
NASA/Goddard Institute for Space Studies	USA	GISS-AOM	(3° × 4°) L12	(3° × 4°) L16
NASA/Goddard Institute for Space Studies	USA	GISS-EH	(4° × 5°) L20	(2° × 2°) L16
NASA/ Goddard Institute for Space Studies	USA	GISS-ER	(4° × 5°) L20	(4° × 5°) L13
Instituto Nazionale di Geofisica e Vulcanologia	Italy	INGV-SXG	T106 (1.125° × 1.125°) L19	(2° × 2°)
Institute for Numerical Mathematics	Russia	INM-CM3.0	(4° × 5°) L21	(2° × 2.5°) L33
Institute Pierre Simon Laplace	France	IPSL-CM4	(2.5° × 3.75°) L19	(2° × 2°) L31
Center for Climate System Research, The University of Tokyo/ National Institute for Environmental Studies/ Frontier Research Center for Global Change (JAMSTEC)	Japan	MIROC3.2(hires)	T106 (–1.1° × 1.1°) L56	(0.2° × 0.3°) L47
Center for Climate System Research, The University of Tokyo/ National Institute for Environmental Studies/ Frontier Research Center for Global Change (JAMSTEC)	Japan	MIROC3.2 (medres)	T42 (–2.8° × 2.8°) L20	(0.5°–1.4° × 1.4°) L43
Meteorological Research Institute	Japan	MRI-CGCM2.3.2	T42 (–2.8° × 2.8°) L30	(0.5°–2.0° × 2.5°) L23
National Center for Atmospheric Research	USA	NCAT_PCM1	T42 (–2.8° × 2.8°) L26	(0.5°–0.7° × 1.1°) L40
Hadley Centre for Climate Prediction and Research/Met Office	UK	UKMO-HadCM3	(2.5° × 3.75°) L19	(1.25° × 1.25°) L20
Hadley Centre for Climate Prediction and Research/Met Office	UK	UKMO-HadGEM1	(–1.3° × 1.9°) L38	(0.3°–1.0° × 1.0°) L40

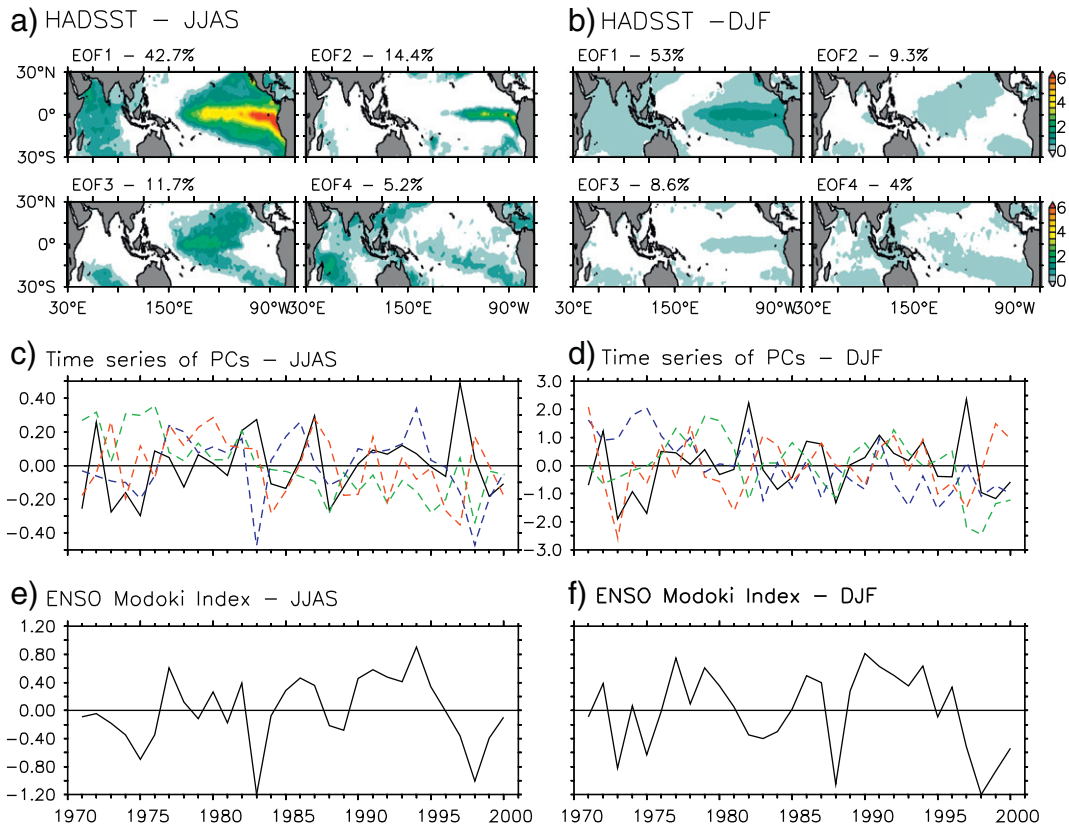


**Fig. 1.** Top four EOF modes of SSTA (a) JJAS (b) DJF for 1971–2000 from observations are shown, with the color shades represented on the bottom. Blue (red) inset rectangle indicates El Niño (Modoki). Time series of PC1 (solid black), PC2 (dash green), PC3 (dash blue), and PC4 (dash red) are shown for (c) JJAS and (d) DJF. Time series of ENSO Modoki index are shown for (e) JJAS (standard deviation = 0.47 °C) and (f) DJF (standard deviation = 0.55 °C).

anthropogenic warming (Ashok et al., 2012). The EOF3 that explains 11.5% of the SST variability captures a zonal tripole pattern in the tropical Pacific region and resembles the ENSO Modoki (Fig. 1a). In the higher latitudes, the positive loadings in the central equatorial Pacific spread eastward in both the hemispheres. The anomalous warming in the central tropical Pacific is flanked by anomalous cooling to its east and west in the El Niño Modoki summers such as 1994 (Fig. 1a and c). Indeed, the correlation between EMI (Figure not shown) and the PC3 is high ( $r = 0.91$ ), and statistically significant at 99% confidence levels, confirming that the mode represents the El Niño Modoki, for boreal summer, during the period under consideration. The EOF2 would have represented El Niño Modoki, had the time period under consideration was from 1979. This is apparent from the PC1 and EMI (Fig. 1), which shows significant correlation during the years from 1971 to 1979. It is to be noted that the Modoki events have become more prominent since early 1980s, and since then are associated with the EOF2 of tropical Pacific variability (Ashok et al., 2007; Kao and Yu, 2009).

During the boreal winter, the EOF1 of the tropical Pacific SSTA captures the ENSO pattern and explains about 53% of the SST variability for the study period (Fig. 1b). ENSO Modoki is represented by the EOF2 that explains 9.3% of the SST variability with SSTA. The EOF3 and EOF4 patterns explain only about 8.6% and 4% of the SST variance, respectively. The time series of the principal components (PCs) of EOF1, EOF2, EOF3 and EOF4 are presented in Fig 1c. The high correlation between PC1 (PC2) and Niño3 (EMI) index is a very high 0.96 (0.73), giving a fairly accurate representation of the conventional El Niño by EOF1 (EOF2), significant above the 99% confidence level from a 2-tailed t-test. The EOF analysis is applied on the simulated tropical Pacific SSTA (see Fig. 2, and Table 2). An examination of the simulated top few modes by the models considers reveals that only ~1/4th of the models from the 20C3M cluster capture the summer and winter ENSO/Modoki as

one of the top three gravest modes. This conclusion is based on the variance explained by the primary EOF modes (Table 2) and an evaluation of the patterns. For example, ENSO being the most important climate driver and the primary mode of the tropical Pacific SST variability, the model variance should be at least comparable to the observations, and at the same time, may not exceed 133% of its observed value, with spatial patterns corresponding to the observations. Strictly speaking, not all the simulated patterns for each model do not exactly match the observations in terms of precise location of the maximums, strength, etc. Even among the more realistic models, the latitudinal width of these captured modes differs from that of the observations. For the JJAS, only 2 out of the 23 models, GFDL-CM2.0 and GFDL-CM2.1, simulate both ENSO and ENSO Modoki as important modes (Fig. 2e, f). INGV-SXG and ECHAM5/MPI-OM capture the ENSO (Fig. 2a, b); CGCM3.1(T47) and CGCM3.1(T63) models are able to capture ENSO Modoki (Fig. 2c, d). The remaining models are not able to reproduce the summer ENSO and ENSO Modoki patterns.

The ENSO and ENSO Modoki patterns during the boreal summer (JJAS) are captured by the simulations of the GFDL-CM2.0 and GFDL-CM2.1 models. The EOF1 pattern of GFDL-CM2.0, for example, captures the ENSO pattern, while explaining 47.08% of the SST variance (Fig. 2e). The eastern warming loading associated with the El Niños, however, is extended westward of dateline, with positive loadings spread in the northern hemisphere. The EOF2 and EOF3 explain 16.32% and 6.56% of the SST variance, respectively. The EOF4 that explains 5.8% of the SST variance (Fig. 2e) looks similar to the observed ENSO Modoki features in the central tropical Pacific region but its latitudinal widths are slightly different from the observations.

The time series of the principal components (PCs) of EOF1, EOF2, EOF3 and EOF4 for the models INGV-SXG, ECHAM5/MPI-OM, CGCM3.1(T47), CGCM3.1(T63), GFDL-CM2.0 and GFDL-CM2.1 for

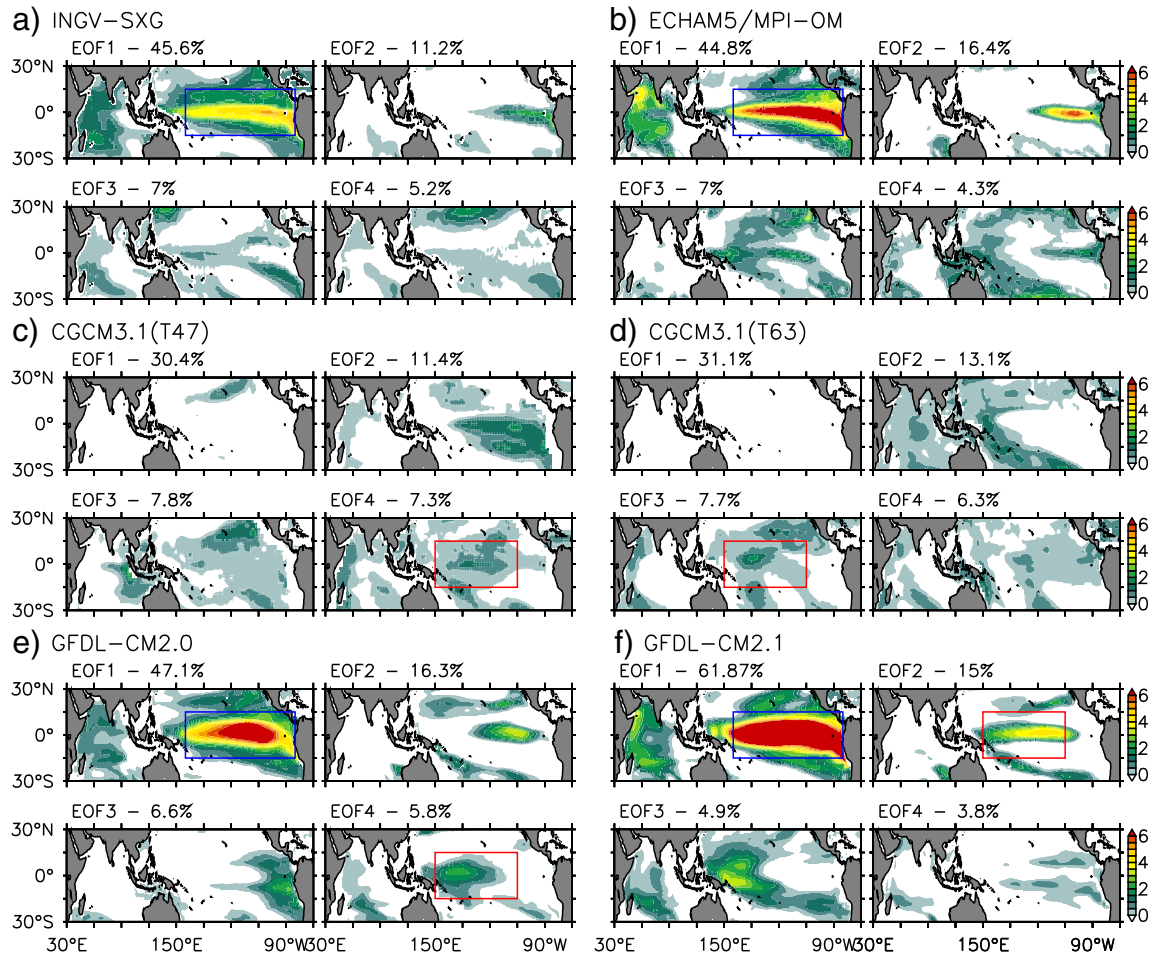


Fig. 2. Top four EOF modes of SSTA-JJAS (20C3M) for the models listed in Table 2. The blue (red) inset rectangle indicates El Niño (Modoki).

JJAS are presented in Fig. 3 and the EMI for the models CGCM3.1(T47), CGCM3.1(T63), GFDL-CM2.0 and GFDL-CM2.1 during the same period are presented in Fig. 4. The simulated Nino3 index correlates well with the PC1 from the GFDL-CM2.0 ( $r=0.97$ ) and EMI correlates with PC4 of the GFDL-CM2.0 at 0.6, (both correlations significant at 99% confidence level from a 2-tailed t-test). The EOF1 pattern of GFDL-CM2.1, on the other hand, captures the ENSO pattern explaining about 61.87% of the SST variance (Fig. 2f), which is an overestimate. The ENSO signature in the eastern Pacific extends westward of the dateline (Fig. 2f) in this model too. The EOF2 that explains 15% of the SST variance captures a pattern similar to ENSO Modoki in the central tropical Pacific with positive (negative) loadings in the northern (southern) hemisphere (Fig. 2f). The EOF2 and EOF3 explain 4.91% and 3.82% of the SST variance respectively. In GFDL-CM2.1, the correlation between Nino3 index and PC1 is 0.98, for conventional ENSO and the correlation between EMI

and PC2 is 0.64, demonstrating the ability to reproduce the ENSO and ENSO Modoki modes.

The INGV-SXG and ECHAM5/MPI-OM models capture the ENSO as a leading mode of boreal tropical Pacific SST variability with a variance of 45.56% and 44.80% respectively (Fig. 2a, b). Once again, the ENSO pattern in the eastern Pacific extends further west as compared to the observations. This common problem was earlier identified by studies such as AchutaRao and Sperber (2006). The Nino3 index and PC1 are highly correlated for INGV-SXG ( $r=0.95$ ) while for ECHAM5/MPI-OM, these are low ( $r=0.38$ ). The EOF2 pattern in the INGV-SXG (ECHAM5/MPI-OM) model explains only about 11.20% (16.43%) of the SST variance. The ENSO Modoki pattern is not captured by these two models in the first four modes while CGCM3.1(T47) (Fig. 2c) and CGCM3.1(T63) (Fig. 2d) capture it by the corresponding EOF4 and EOF3 modes that explain a variance of 7.26% and 7.66%, respectively. This can be also ascertained by the fact that in the CGCM3.1(T47), EMI is correlated with PC4 ( $r=0.75$ ) and in CGCM3.1(T63), it is correlated with PC3 ( $r=0.84$ ). The remaining models fail to reproduce ENSO and ENSO Modoki patterns (Table 2). In EOF4 of CGCM3.1(T47), the central Pacific loadings are seen to spread eastward of tropical Pacific in higher latitudes in the northern hemisphere, and westward of tropical Pacific in the southern hemisphere. In EOF3 of CGCM3.1(T63), in higher latitudes, the positive loadings in the central equatorial Pacific spread eastward in northern hemisphere and southward in southern hemisphere. The EOF1, EOF2 and EOF3 patterns of CGCM3.1(T47) explain about 30.40%, 11.40% and 7.79% of the SST variance. The EOF1, EOF2 and EOF4 patterns of CGCM3.1(T47) explain about 31.05%, 13.09% and 6.33% of the SST variance, respectively.

Table 2

Categorization of simulated ENSO flavors in 20C3M for boreal summer season (JJAS). \* represents ENSO and # represents ENSO Modoki in the corresponding mode of EOF.

Models in 20C3M (JJAS)	EOF modes and corresponding variance explained (%)			
	EOF 1	EOF 2	EOF 3	EOF 4
INGV-SXG	45.56*	11.20	6.96	5.20
ECHAM5/MPI-OM	44.80*	16.43	6.89	4.33
CGCM3.1(T47)	30.38	11.38	7.79	7.26#
CGCM3.1(T63)	31.05	13.09	7.66#	6.33
GFDL-CM2.0	47.08*	16.32	6.56	5.80#
GFDL-CM2.1	61.87*	15.04#	4.91	3.82

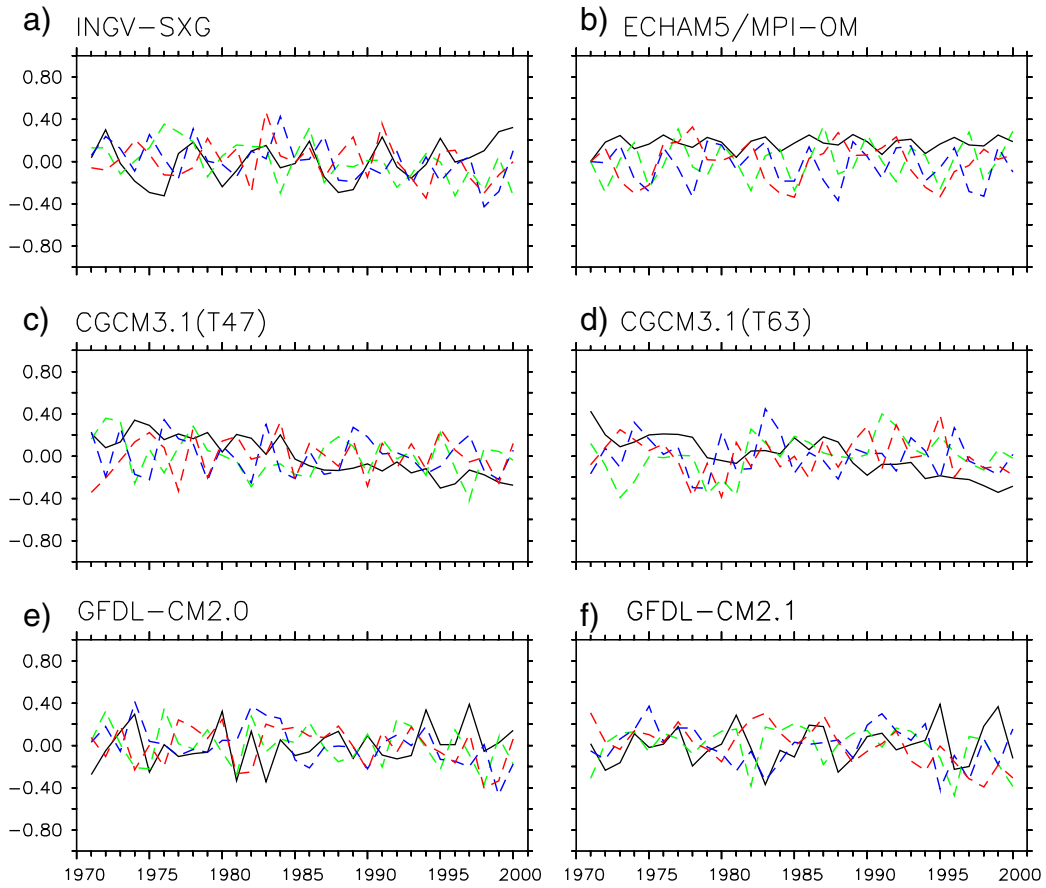


**Fig. 3.** Time series of PC1 (solid black), PC2 (dash green), PC3 (dash blue), and PC4 (dash red) for the models in JJAS 20C3M (a) INGV-SXG (b) ECHAM5/MPI-OM (c) CGCM3.1(T47) (d) CGCM3.1(T63) (e) GFDL-CM2.0 and (f) GFDL-CM2.1.

Since the current study examines the teleconnections between ENSO/Modoki and the Indian summer monsoon, it is important to examine how well the model simulates the Indian summer monsoon climate. Fig. 5 shows the mean precipitation for June–September over the monsoon region, in the model and the observations. The mean

patterns of the observed monsoon precipitation over the land appear to be reasonably simulated in the models INGV-SXG, ECHAM5/OPA-OM, GFDL CM2.0 and GFDL CM 2.1. The precipitation over the Western Ghats and the Ganges Basin regions is reproduced in these models though the magnitude of precipitation is weak, which is a shortcoming

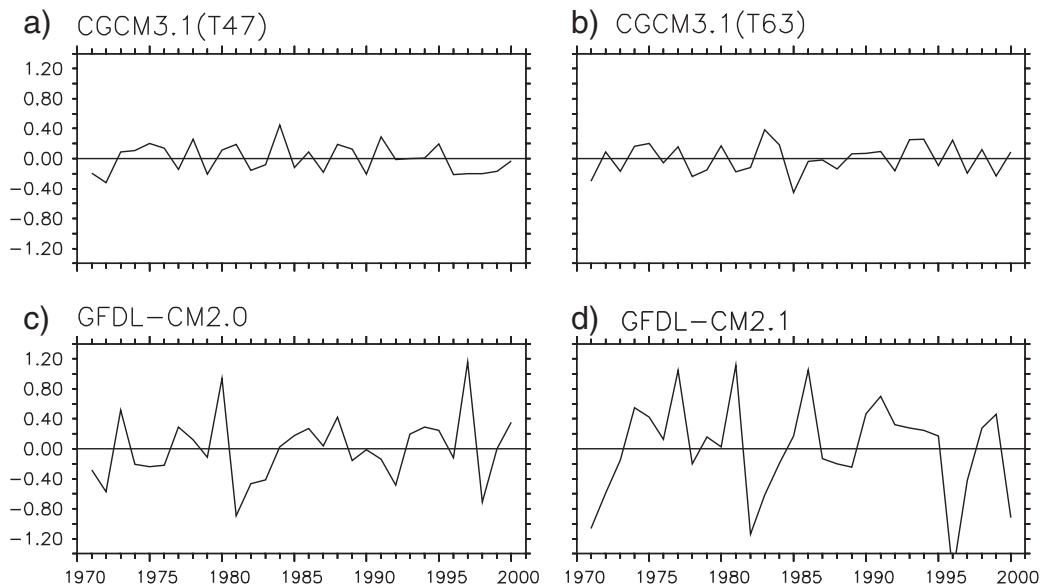


**Fig. 4.** Time series of ENSO Modoki index (standard deviation) (a) CGCM3.1(T47) (0.19 °C) (b) CGCM3.1(T63) (0.19 °C) (c) GFDL-CM2.0 (0.44 °C) and (d) GFDL-CM2.1 (0.65 °C) for JJAS in 20C3M.

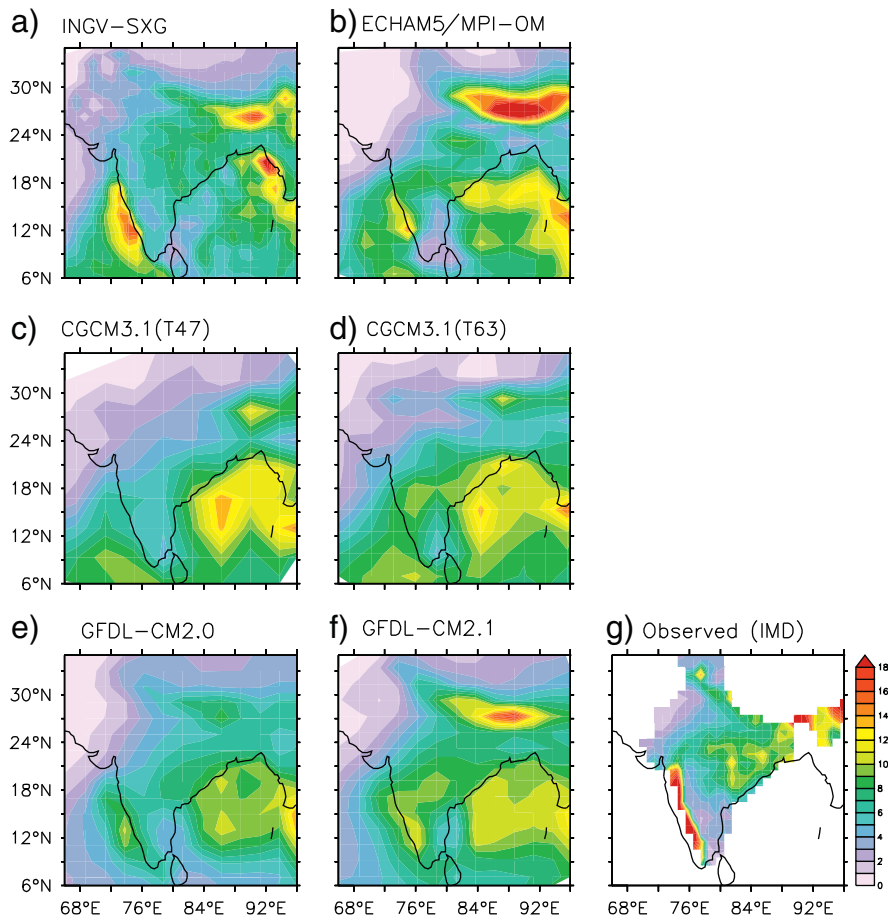


**Fig. 5.** Climatology of precipitation (colors;  $\text{mm day}^{-1}$ ) over the Asian monsoon region during June–September, for (a to f) the models and (g) the observations. Shading conventions are represented at the side of the last figure.

common to many GCMs (Roxy et al., in press). This gives us some confidence in these models, for investigating the evolution of ENSO/Modoki–monsoon teleconnections in a changing climate.

### 3.2. The ENSO and ENSO Modoki in the SRESA1B scenario

To evaluate the potential role of the global warming in modulating the frequency of the ENSOs and ENSO Modokis, the ENSO and Modoki variability as simulated by the SRESA1B scenario of the GFDL-CM2.0 and GFDL-CM2.1 models are examined. These models are selected as their 20C3M realizations have a moderate but at least qualitatively realistic representation of the ENSO and Modoki patterns in the 20C3M, and successfully capture the temporal evolution. The ENSO (ENSO Modoki) still appears as the primary (secondary) mode with slight changes in the variance. However, the GFDL-CM2.0 portrays remarkable change in the mode and variance of Modoki. In the 20C3M simulations, for example, the Modoki is associated with the EOF4 with 6% variance, while in the SRESA1B it goes up as the 2nd mode explaining a 12% of the tropical Pacific SST variance. This indicates an increasing prominence of Modoki events in a global warming scenario.

The PC1 of the GFDL-CM2.0 and the corresponding simulated Nino3 index have a high correlation ( $r=0.9$ ), indicating that EOF1 represents the ENSO. The EOF1 pattern explains 59% of the tropical Pacific SST variance (Fig. 6a). The westward extension issue still persists, indicating that this is “probably” a systematic bias. The correlation for the model between PC2 and EMI appears reasonable ( $r=0.67$ ). The EOF2, explaining 12% of the SST variance, captures a pattern similar to ENSO Modoki in the central tropical Pacific region but its

latitudinal widths are slightly different from the observations, with positive loadings seen at higher latitudes of northern hemisphere (Fig. 6b).

In the case of GFDL-CM2.1, the ENSO is portrayed by the EOF1 mode that captures about 58.70% of the SST variance (Fig. 2), with a high correlation between PC1 and Nino3 index ( $r=0.9$ ). The EOF2 resembles the Modoki structure, and explains 8.77% of the tropical SST variance, with a reasonable correlation ( $r=0.56$ ) between PC2 and EMI. However, it is to be noted that the variance explained by the EOF2 in GFDL-CM2.1 has gone down from 15% in the 20C3M simulations to 9% in the SRESA1B. Since the two models (GFDL CM2.0 and CM2.1) show a difference in the change of variance for SRESA1B with respect to the 20C3M simulations, the teleconnection patterns might also vary accordingly, which are discussed in Section 4.

### 3.3. Teleconnections between ENSO/Modoki and the Indian summer monsoon

ENSO and, more recently the ENSO Modoki, are two major drivers of the Indian summer monsoon rainfall distribution (ISMR; Ashok et al., 2007; Kumar et al., 2006; Ropelewski and Halpert, 1987). Therefore, it is important to evaluate any changing teleconnections between these drivers and the ISMR in light of the ability of the models to reproduce these drivers, in addition to their skills in capturing the ISMR variability. Partial correlations between the Nino3 index and the gridded summer monsoon rainfall anomalies over the Indian region with the rainfall for the boreal summers starting from 1971 through 2000, after removing the linear influence of EMI index, are presented in Fig. 7a. Significant negative correlations are observed in north and western India. Similarly, the partial correlations of observed data between rainfall anomalies

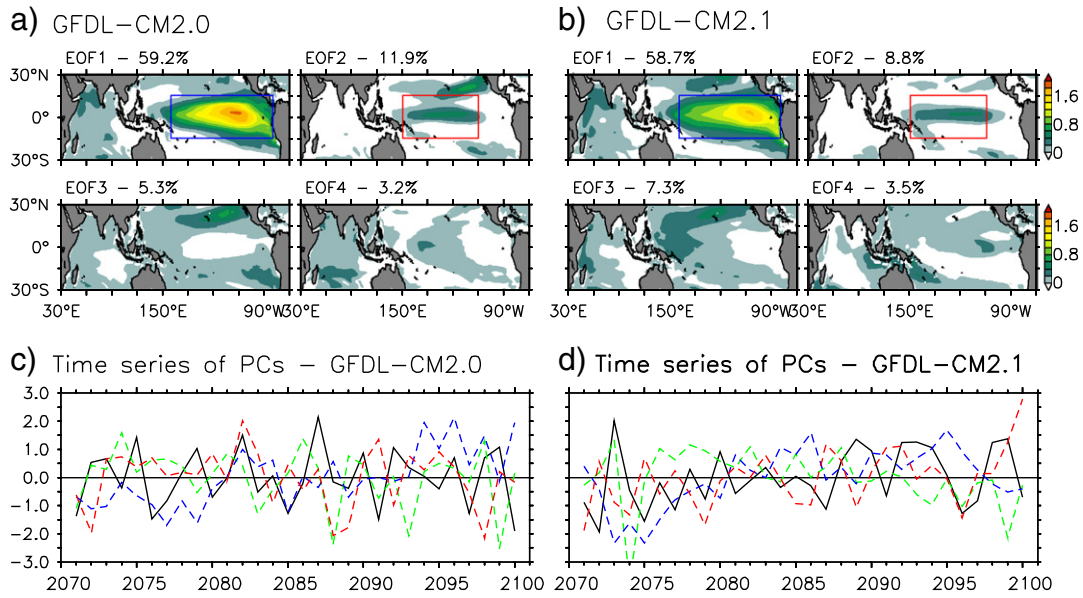


**Fig. 6.** Top four EOF modes of SSTA-JJAS (SRESA1B) for GFDL-CM2.0 and GFDL-CM2.1. The blue (red) inset rectangle indicates El Niño (Modoki). Time series of PC1 (solid black), PC2 (dash green), PC3 (dash blue), PC4 (dash red) are shown for (c) GFDL-CM2.0 and (d) GFDL-CM2.1.

with EMI for the same period, after removing the linear influence of Nino3 index are presented in Fig. 7b. The analysis reconfirms a significant influence of the ENSO Modoki events on the ISMR distribution. Significant negative correlations are seen in the parts of the western ( $r = -0.3$ ), southern ( $r = -0.4$ ) and northeastern ( $r = -0.3$ ) regions of the Indian subcontinent, at 95% confidence levels. Positive correlations ( $r = 0.3$ ) are seen over the central-eastern India.

A similar analysis is carried out on the two selected models to assess their ability in reproducing the observed interrelationship between ENSO/ENSO Modoki and ISMR for the 1971–2000 period. A correlation analysis between ISMR and Nino3 in the GFDL-CM2.1 shows unrealistic strong positive correlations from central to north of India (Fig. 8d). The results from the GFDL-CM2.0 model, on the other hand, show (Fig. 8c) negative correlations, which is in agreement with observations. Having said that, the magnitude of the correlations is stronger than that from the observations. The partial correlation between the EMI and rainfall anomalies for the models GFDL-CM2.0 and GFDL-CM2.1 is shown in Fig. 8a and b. The model GFDL-CM2.0 successfully captures the observed negative correlations between the ISMR

and EMI, over the south of India but fails to capture the positive correlations further north (Fig. 7a). However, the signs of the partial correlation of the EMI with ISMR, as simulated by the model GFDL-CM2.1, are opposite to that from the observations.

To investigate the influence of climate change on the ENSO/ENSO Modoki-ISMIR relationship, the seasonal precipitation obtained from the climate change experiment SRESA1B is examined using partial correlation techniques. The JJAS partial correlations computed between the Nino3 and rainfall anomalies for the GFDL-CM2.0 and GFDL-CM2.1 models are shown in Fig. 9c and d. The GFDL-CM2.0 model exhibits significant positive correlation over the northeast of Indian subcontinent, which indicates surplus rainfall over that region during a positive ENSO event (Fig. 9c). The northwest and the southern regions also demonstrate a similar positive correlation while the rest of the subcontinent shows a weak negative correlation. This indicates an inconsistency with the current day simulations as well as with that from the observations. Interestingly, the overall correlations from the GFDL-CM2.1 model are significantly negative, with strong negative correlations ( $r = -0.5$ ) in central to southern part of the subcontinent, indicating the deficient

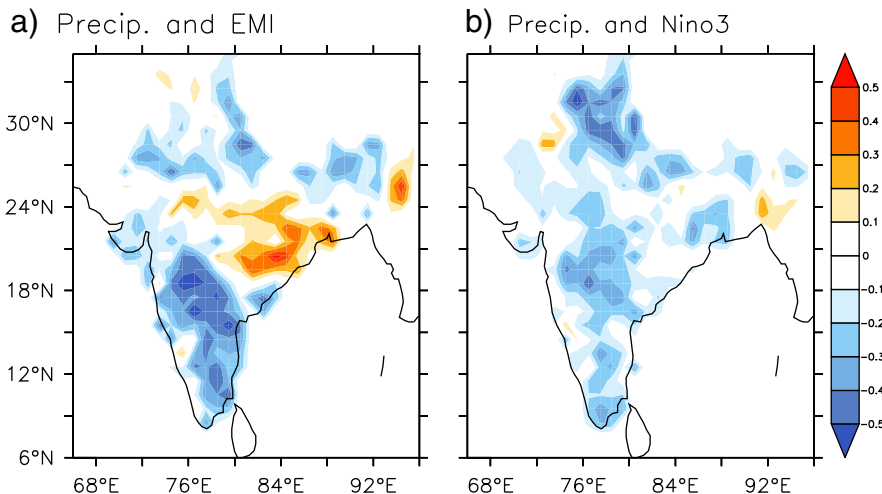


**Fig. 7.** (a) JJAS (1971–2000) partial correlations between observed rainfall anomalies and corresponding EMI (b) same as Fig. 6a but with Nino3 index.

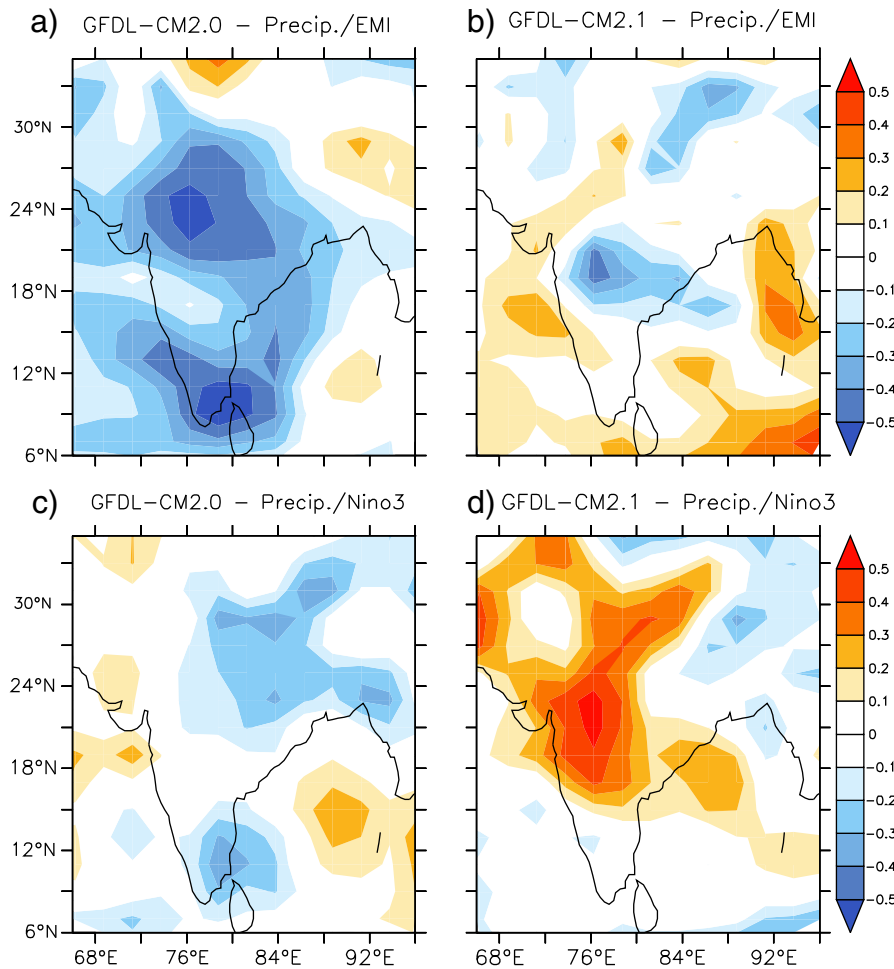


**Fig. 8.** Partial correlations between rainfall anomalies and corresponding EMI, with linear effects of Nino3 SST removed, for (a) GFDL-CM2.0 and (b) GFDL-CM2.1 for JJAS in 20C3M. Partial correlations with Nino3 index are shown in (c) GFDL-CM2.1 and (d) GFDL-CM2.0.

rainfall during an El Niño event (Fig. 9d). The monsoon–ENSO relationship in the SRESA1B simulations by both the models is completely opposite to the corresponding 20C3M simulations.

The partial correlations computed between the EMI and rainfall anomalies for the models GFDL-CM2.0 and GFDL-CM2.1 for the study period in SRESA1B are shown in Fig. 9a and b. The model GFDL-CM2.0 exhibits positive correlations over north and northeast and negative correlations over the southern part of the Indian subcontinent. The ENSO Modoki and ISMR relationship is well simulated by the model GFDL-CM2.1 in many parts of the subcontinent (Fig. 9b).

#### 4. Discussion and concluding remarks

Data from the observations, and that from the 20C3M and SRESA1B climate change runs from the IPCC AR4 were analyzed to study whether the IPCC climate models can reproduce the ENSO and ENSO Modoki patterns as the gravest two modes from statistical linear analysis, as observed, and their teleconnections with the Indian summer monsoon, and also the implications for the future. An EOF analysis of the observational SST anomalies in the tropical Pacific shows that the El Niño and El Niño Modoki explain 45% and 13% of the tropical Pacific SST variance respectively for the boreal summer season during the period from 1971 through 2000, in broad agreement with Ashok et al. (2007). It is found that only 1/4th of the models from 20C3M capture either ENSO or ENSO Modoki pattern in JJAS. Of this 1/4th, only the GFDL-CM2.0 and GFDL-CM2.1 models simulate both ENSO and ENSO Modoki as important modes in JJAS. Furthermore, only one model, GFDL-CM2.0,

simulates both ENSO and ENSO Modoki as important modes during both summer and winter. In summary, only the GFDL-CM2.0 model captures both the Modoki and ENSO modes realistically for boreal summer as well as boreal winter during the last 30 years of the 20C3M.

Yeh et al. (2009) and Ashok and Yamagata (2009) suggested that the frequent occurrence of the El Niño Modoki events since late 1970s is due to global warming. Yeh et al. (2009) analyzed the statistics of the representative indices of the ENSO Modoki and ENSO from the 20C3M and SRESA1B outputs, and suggested that the ENSO Modoki events may indeed increase in a global warming condition. However, the current analysis indicates that at a more fundamental modal level, which involves not just the temporal frequency but also the spatial distributions, the models (i) still fail to capture these modes and that there is no consistent agreement within the models, and (ii) that due caution, and further analysis, is necessary to conclude anything from the AR4 projections about the frequency modulation of the ENSO flavors by the global warming signal.

Observational analysis for the period 1971–2000 shows that the ENSO Modoki has stronger impact as compared to that of the ENSO, in agreement with Kumar et al. (2006) and Ashok et al. (2007). Interestingly, Kripalani et al. (2007) and Sabade et al. (2011), based on the IPCC AR4 data analysis, broadly suggest that the monsoon–ENSO relationship does not change noticeably. From the present study, it is deciphered that the two models that reproduce ENSO Modoki as well as ENSO associated variance in both 20C3M and SRESA1B represent the links of the ISMR with ENSO reasonably in 20C3M, but indicate opposite type of impacts in SRESA1B. With the limited skills

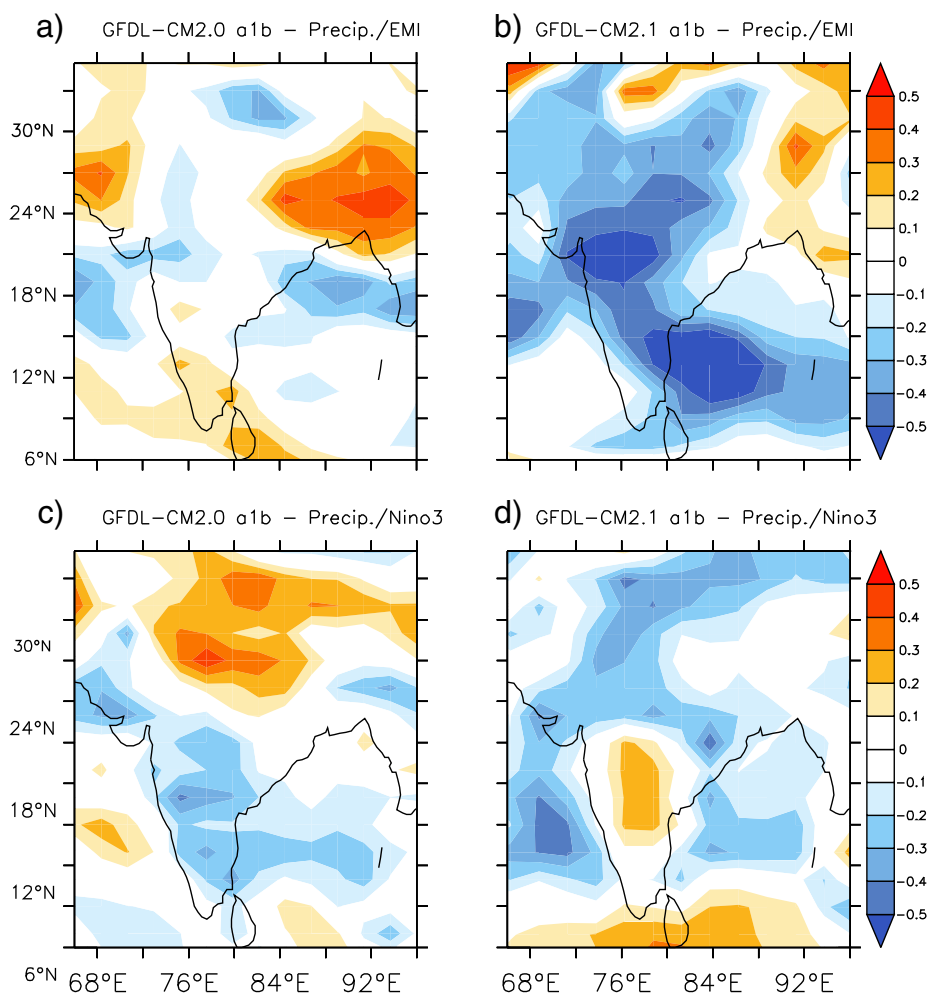


**Fig. 9.** Partial correlations between rainfall anomalies and Nino3 index from (a) GFDL-CM2.0 (b) GFDL-CM2.1 for JJAS in SRESA1B. Partial correlations with EMI are shown in (c) GFDL-CM2.0 and (d) GFDL-CM2.1.

of the models in reproducing the monsoon, the ENSO and ENSO Modoki, it is difficult to reconcile that the teleconnections of a tropical driver can change like that. The model GFDL-CM2.1 expresses the expected negative correlations from tropical Pacific on the Indian summer monsoon in SRESA1B scenarios, but it is unable to reproduce the observed links during the 20th century. This issue, as discussed in Section 3.2, might be due to the fact that variances of the leading modes are simulated differently in both of GFDL models. All these indicate the challenges associated with the limitations of the models in reproducing the variability of the monsoons and ENSO flavors, not to speak of failing in capturing the potential impacts of global warming as they are expected to. More research in improving the current day simulations, improving model capacity to simulate better by improving the Green House Gases (GHG) and aerosols in the models are some of the important and immediate steps that are necessary. Probably, the IPCC AR5 array, with better model physics and innovative Representative Concentration Pathway (RCP) designing, may provide an opportunity to look into these issues.

### Acknowledgments

The authors acknowledge the role of the international modeling community and the Program for Climate Model Diagnostic and Intercomparison for making the data available. The study was facilitated by the Indian Institute of Tropical Meteorology, Ministry of Earth

Sciences, India. K.As. conceived the study; N.P. did the data analysis; R.M. and K.As. wrote the manuscript; R.M. and K.Ap. plotted the figures.

### References

- AchutaRao, K., Sperber, K.R., 2006. ENSO simulation in coupled ocean–atmosphere models: are the current models better? *Climate Dynamics* 27 (1), 1–15.
- Annamalai, H., Hamilton, K., Sperber, K.R., 2007. The South Asian summer monsoon and its relationship with ENSO in the IPCC AR4 simulations. *Journal of Climate* 20 (6), 1071–1092.
- Ashok, K., Yamagata, T., 2009. The El Niño with a difference? *Nature* 461, 481–484. <http://dx.doi.org/10.1038/461481a>.
- Ashok, K., Behera, S.K., Rao, S.A., Weng, H.Y., Yamagata, T., 2007. El Niño Modoki and its possible teleconnection. *Journal of Geophysical Research-Oceans* 112 (C11).
- Ashok, K., Sabin, T.P., Swapna, P., Murtugudde, R.G., 2012. Is a global warming signature emerging in the tropical Pacific? *Geophysical Research Letters* 39 L02701. <http://dx.doi.org/10.1029/2011GL050232>.
- Bretherton, C.S., Smith, C., Wallace, J.M., 1992. An intercomparison of methods for finding coupled patterns in climate data. *Journal of Climate* 5, 541–560.
- Collins, W., et al., 2006. Radiative forcing by well-mixed greenhouse gases: estimates from climate models in the Intergovernmental Panel on Climate Change (IPCC) Fourth Assessment Report (AR4). *Journal of Geophysical Research* 111 (D14317), 1–2.
- Kao, H.Y., Yu, J.Y., 2009. Contrasting eastern-Pacific and central-Pacific types of ENSO. *Journal of Climate* 22 (3), 615–632.
- Kripalani, R., Oh, J., Kulkarni, A., Sabade, S., Chaudhari, H., 2007. South Asian summer monsoon precipitation variability: coupled climate model simulations and projections under IPCC AR4. *Theoretical and Applied Climatology* 90 (3), 133–159.
- Kug, J.S., Jin, F.F., An, S.I., 2010. Two types of El Niño events: cold tongue El Niño and warm pool El Niño.
- Kumar, K.K., Rajagopalan, B., Hoerling, M., Bates, G., Cane, M., 2006. Unraveling the mystery of Indian monsoon failure during El Niño. *Science* 314 (5796), 115.
- Levitus, S., Antonov, J., Boyer, T., 2005. Warming of the world ocean, 1955–2003. *Geophysical Research Letters* 32 (2).

- McPhaden, M.J., et al., 1988. The response of the equatorial Pacific Ocean to a westerly wind burst in May 1986. *Journal of Geophysical Research* 93 (C9), 10589–10,603.
- Meehl, G.A., et al., 2007. The WCRP CMIP3 multimodel dataset. *Bulletin of the American Meteorological Society* 88, 1383–1394.
- Rajeevan, M., Bhate, J., Kale, J., Lal, B., 2006. High resolution daily gridded rainfall data for the Indian region: analysis of break and active monsoon spells. *Current Science* 91 (3), 296–306.
- Rasmusson, E.M., Carpenter, T.H., 1982. Variations in tropical sea surface temperature and surface wind fields associated with the Southern Oscillation/El Niño. *Monthly Weather Review* 110 (5), 354–384.
- Rasmusson, E.M., Carpenter, T.H., 1983. Relationship between eastern equatorial Pacific sea surface temperatures and rainfall over India and Sri Lanka. *Monthly Weather Review* 111 (3).
- Rayner, N., et al., 2003. Global analyses of sea surface temperature, sea ice, and night marine air temperature since the late nineteenth century. *Journal of Geophysical Research* 108 (D14), 4407.
- Ropelewski, C.F., Halpert, M.S., 1987. Global and regional scale precipitation patterns associated with the El Niño/Southern Oscillation. *Monthly Weather Review* 115 (8), 1606–1626.
- Roxy, M., Gualdi, S., Drbohlav, H.-K., Navarra, A., 2011. Seasonality in the relationship between El Niño and Indian Ocean dipole. *Climate Dynamics* 37 (1), 221–236.
- Roxy, M., Tanimoto, Y., Preethi, B., Pascal, T., Krishnan, R., in press. Intraseasonal SST-precipitation relationship and its spatial variability over the tropical summer monsoon region. *Climate Dynamics*. <http://dx.doi.org/10.1007/s00382-012-1547-1>.
- Sabade, S., Kulkarni, A., Kripalani, R., 2011. Projected changes in South Asian summer monsoon by multi-model global warming experiments. *Theoretical and Applied Climatology* 1–23.
- Shukla, J., 1987. Interannual variability of monsoons. *Monsoons*.
- Yeh, S.W., et al., 2009. El Niño in a changing climate. *Nature* 461 (7263), 511–514.